Contrib Mineral Petrol (2007) 153:177–190
DOI 10.1007/s00410-006-0139-7

ORIGINAL PAPER

# Tracing magma mixing in granite genesis: in situ U–Pb dating and Hf-isotope analysis of zircons

**Jin-Hui Yang · Fu-Yuan Wu · Simon A. Wilde · Lie-Wen Xie · Yue-Heng Yang · Xiao-Ming Liu**

Received: 25 December 2005 / Accepted: 17 August 2006 / Published online: 20 September 2006


**Abstract** In situ zircon U–Pb and Hf-isotopic data have been determined for mafic microgranular enclaves and host granitoids from the Early Cretaceous Gudaoling batholith in the Liaodong Peninsula, NE China, in order to constrain the sources and petrogenesis of granites. The zircon U–Pb age of the enclaves (120 ± 1 Ma) is identical to that of the host monzogranite (120 ± 1 Ma), establishing that the mafic and felsic magmas were coeval. The Hf isotopic composition of the enclaves [$\varepsilon_{Hf}(t)$ = +4.5 to –6.2] is distinct from the host monzogranite [$\varepsilon_{Hf}(t)$ = –15.1 to –25.4], indicating that both depleted mantle and crustal sources contributed to their origin. The depleted mantle component was not previously revealed by geochemical and Nd and Sr isotopic studies, showing that zircon Hf isotopic data can be a powerful geochemical tracer with the potential to provide unique petrogenetic information. Some wall-rock contamination is indicated by inherited zircons with considerably older U–Pb ages and low initial Hf isotopic compositions. Hafnium isotopic variations in Early Cretaceous zircons rule-out simple crystal–liquid fractionation or restite unmixing as the major genetic link between enclaves and host rocks. Instead, mixing of mantle-derived mafic magmas with crustal-derived felsic magmas, coupled with assimilation of wall rocks, is compatible with the data.

Communicated by T.L. Grove.

**Electronic supplementary material** Supplementary material is available in the online version of this article at http://dx.doi.org/10.1007/s00410-006-0139-7 and is accessible for authorized users.

J.-H. Yang (✉) · F.-Y. Wu · L.-W. Xie · Y.-H. Yang
State Key Laboratory of Lithospheric Evolution,
Institute of Geology and Geophysics,
Chinese Academy of Sciences,
P.O. Box 9825, Beijing 100029, China
e-mail: jinhui@mail.igcas.ac.cn

S. A. Wilde
Department of Applied Geology,
Curtin University of Technology,
P.O. Box U1987, Perth, WA 6845, Australia

X.-M. Liu
Key Laboratory of Continental Dynamics,
Department of Geology, Northwest University,
Xi'an 750069, China

## Introduction

Magma mixing has been widely recognized from field observations, whole rock geochemistry and Nd and Sr isotopic data in both plutonic and volcanic environments (Holden et al 1987; Eberz et al. 1990; Kepezhinskas et al. 1997; Keay et al. 1997; Snyder and Tait 1998; Clynne 1999; Millar et al. 2001; Kemp and Hawkesworth 2003; Yang et al. 2004a; Bonin 2004). The basis of such interpretations is the recognition of the primitive sources of basic and acid magmas. However, identifying the specific sources that contributed to the origin of granitoids has long been a problem, since both magma mixing and wall-rock assimilation can significantly modify the rock chemistry. This can result in homogeneous Nd and Sr isotopic compositions in what were initially discrete components within a single pluton or batholith (Lesher 1990; Poli et al. 1996; Barbarin 2005).

Zircon, a ubiquitous accessory mineral in both granites and enclosed microgranular enclaves, is extremely resistant to later geological processes and can survive post-crystallization thermal disturbances (Pidgeon and Aftalion 1978; Elburg 1996; Kinny and Maas 2003). It is a mineral well suited not only for U–Pb dating, but also for hafnium isotopic studies, because zircon has high hafnium concentrations and low Lu/Hf ratios, so that correction for in situ radiogenic growth is negligible. Furthermore, the Lu–Hf isotopic system can be utilized to track the history of chemical differentiation of the Earth (crust and mantle) by virtue of the fact that fractionation of Lu from Hf occurs during magma generation (Kinny et al. 1991). Recent studies show that hafnium isotopic compositions of zircon can elucidate the nature of magma sources and the role of magma mixing processes in the generation of granitoids (Griffin et al. 2002; Wang et al. 2003; Kemp and Hawkesworth 2006; Yang et al. 2006a).

Mafic microgranular enclaves (MMEs, see review of Didier and Barbarin 1991) are common in intermediate to felsic granitoids and can provide significant information on the nature of the source rocks, the mechanism of production of granitic melt, as well as evidence of interaction between continental crust and mantle. However, there are considerable discrepancies between the models proposed to explain the origin of MMEs, including whether they are restites (Chappell et al. 1987; Chappell and Stephens 1988; Chen et al. 1989; Chappell 1997; White et al. 1999; Chappell et al. 2000), inclusions of basic magma derived from the mantle (Eichelberger 1980; Vernon 1984; Holden et al. 1987; Vernon et al. 1988; Yang et al. 2004a; Bonin 2004; Yang et al. 2006a) or derived from mafic rocks in the lower crust (Kepezhinskas et al. 1997; Maas et al. 1997). Here we report in situ U–Pb and Hf isotopic data for zircons from mafic microgranular enclaves, the host granite and also from the wall rock of the granite (Archean gneiss—the predominant basement rock in the study area) for the Early Cretaceous Gudaoling batholith in NE China. We use these data to identify the origin of the mafic microgranular enclaves and to constrain the possible sources and potential magma mixing in the granite.

## Geological setting

The Liaodong Peninsula forms the northeastern segment of the North China Craton (NCC, Fig. 1a) and consists of Archean to Paleoproterozoic basement rocks overlain by unmetamorphosed Mesoproterozoic to Paleozoic sediments and Mesozoic to Cenozoic sedimentary and volcanic rocks. Deformed Late Archean gneisses have diorite, tonalite and granodiorite protoliths, with ages of ~2,500 Ma (LBGMR 1989). In the Paleoproterozoic, the Liaohe Group was deposited and then metamorphosed during the 1.85 Ga collisional event that is considered to mark cratonization of the NCC (Zhao et al. 2001, 2005). Subsequently, the Liaodong Peninsula was covered by a thick sequence of Meso- to Neo-proterozoic and Paleozoic sediments. Paleozoic diamond-bearing kimberlite, Late Triassic dolerite, diorite, monzogranite, nepheline syenite and Cenozoic gabbro are also present in the Liaodong Peninsula (Yang et al. 2004b; Wu et al. 2005a, b). In the Mesozoic, about 20,000 $km^2$ of intrusive rocks were emplaced, along with minor volcanic rocks (Wu et al. 2005a). Detailed zircon U–Pb dating shows that Mesozoic magmatism can be divided into three phases: (1) Late Triassic syenites, dolerites and monzogranites (220–212 Ma) (Yang et al. 2004b), (2) Jurassic granites (179–156 Ma), consisting of hornblende-bearing tonalite–granodiorite and two-mica monzogranite (Wu et al. 2005b) and (3) Early Cretaceous (131–117 Ma), dolerite, diorite, granodiorite, monzogranite, syenogranite, A-type granite and syenite (Yang et al. 2004a; Wu et al. 2005a; Yang et al. 2006a).

The Cretaceous Gudaoling batholith is one of the early Cretaceous intrusions (Yang et al. 2004a; Wu et al. 2005a) in the Liaodong Peninsula and consists mainly of monzogranite with abundant enclaves (Fig. 1b, c). The monzogranite is composed of plagioclase (39–43%), alkali-feldspar (24–29%), quartz (19–35%) and biotite (5%), with or without hornblende (1–3%). Accessory minerals include apatite, zircon, titanite and Fe–Ti oxides. The microgranular enclaves mostly range from angular to oval in shape (Fig. 1c), but locally form dyke-like trails that progressively thin toward their terminations with the host granitoid. They range in composition from diorite to quartz diorite (Yang et al. 2004a). Igneous textures include oscillatory-zoned plagioclase, local quartz and K-feldspar megacrysts and some myrmekitic intergrowths between plagioclase and alkali feldspar (Yang et al. 2004a), identical to textures described from mafic enclaves around the world (Eichelberger 1980; Vernon 1984; Holden et al. 1987; Vernon et al. 1988; Didier and Barbarin 1991). In addition, several of the enclaves are themselves host to granitic material, some of which is entirely enclosed within diorite.

Detailed geochemical and Sr–Nd isotopic analyses (Yang et al. 2004a) show that the enclaves have high contents of MgO (Mg# up to 72), Cr (max. 493 ppm), Ni (max. 181 ppm) and low silica contents ($SiO_2$ 51–60 wt%), indicating derivation from a mantle source distinct from the granites, which have the signature of a

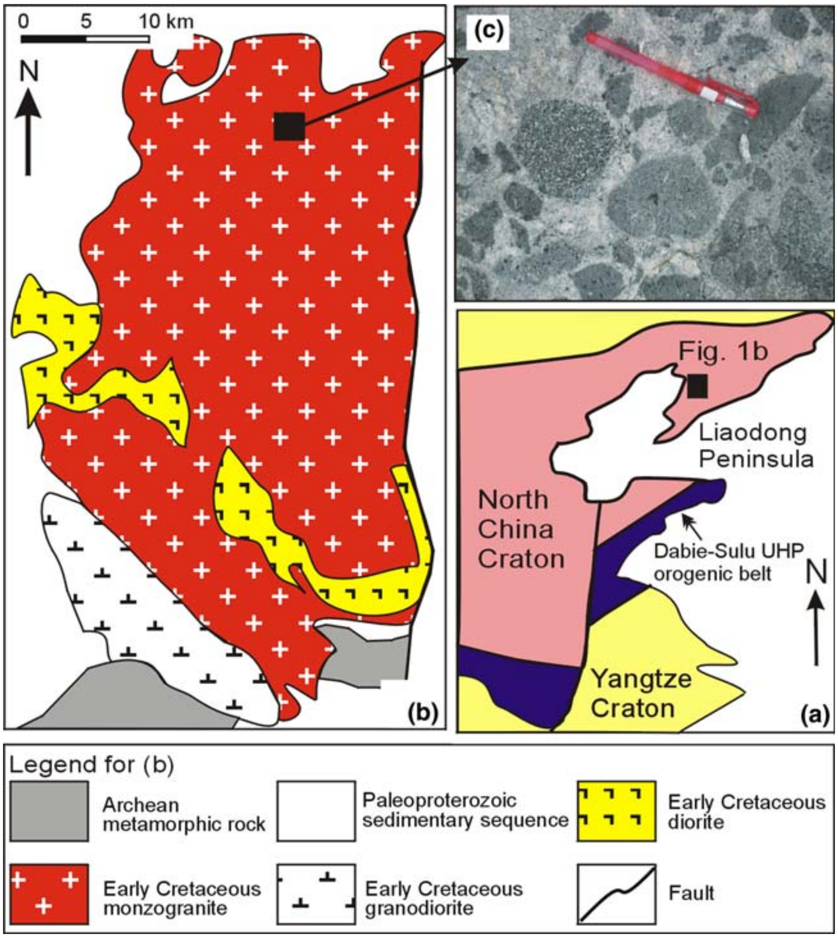


**Fig. 1** **a** Simplified geological map showing location of Liaodong Peninsula and study area in the North China Craton; **b** Geological map of the Gudaoling batholith in the Liaodong Peninsula and **c** Mafic microgranular enclaves occurring within monzogranite. The pen in **c** is 14 cm long

crustal melt, i.e., high $SiO_2$ (68.4–72.6 wt%), and low MgO (0.16–0.87 wt%), Cr (3.6–7.8 ppm) and Ni (1.9–4.8 ppm) contents. The enclaves are enriched in light rare earth (LREE) and large ion lithophile (LILE) elements and depleted in the high field strength elements (HFSE) (Fig. 2). They have initial $^{87}Sr/^{86}Sr$ ratios of 0.7058–0.7073 and negative $\varepsilon_{Nd}(t)$ values ranging from –7.2 to –17.6. However, the geochemical features of the mafic microgranular enclaves cannot be explained either as melts derived from an enriched mantle source (lithospheric mantle metasomatised by recycled crustal materials) or as melts derived from depleted (asthenospheric) mantle with crustal contamination, since they are affected by magma mixing and do not represent primitive melts.

## Analytical methods

One host monzogranite, one wall-rock (gneiss) and five MME samples from the Gudaoling batholith were chosen for zircon U–Pb dating and Hf isotopic analyses. Major and trace element analyses (Table 1) show that the five enclaves are mafic to intermediate in composition ($SiO_2$ 53.4–63.0 wt.%) and have a high Mg# (62.2–67.0). The monzogranite has a high $SiO_2$ content (73.0 wt.%) and low Mg# (~29.2). Both enclaves and host rocks have high total REE contents and are enriched in LREE. In the primitive mantle (PM)-normalized trace element diagram (Fig. 2b), all of these rocks are enriched in LILEs, such as Rb, Ba, Sr and LREEs, and depleted in HFSEs, such as Nb, Ta, P, Ti.

Cathodoluminescence (CL) images were obtained using a CAMECA SX–50 microprobe at the Institute of Geology and Geophysics, Chinese Academy of Sciences in Beijing, in order to characterize the internal structures of the zircons and to choose potential target sites for U–Pb dating and Hf analyses.

Laser ablation ICP-MS zircon U–Pb analyses were conducted on an Agilent 7500a ICP-MS equipped with a 193 nm laser, which is housed at the Department of Geology, Northwest University in Xi'an, China. During analysis, the spot diameter was 30 μm. Raw count rates for $^{29}Si$, $^{204}Pb$, $^{206}Pb$, $^{207}Pb$, $^{208}Pb$, $^{232}Th$ and $^{238}U$ were collected for age determination.

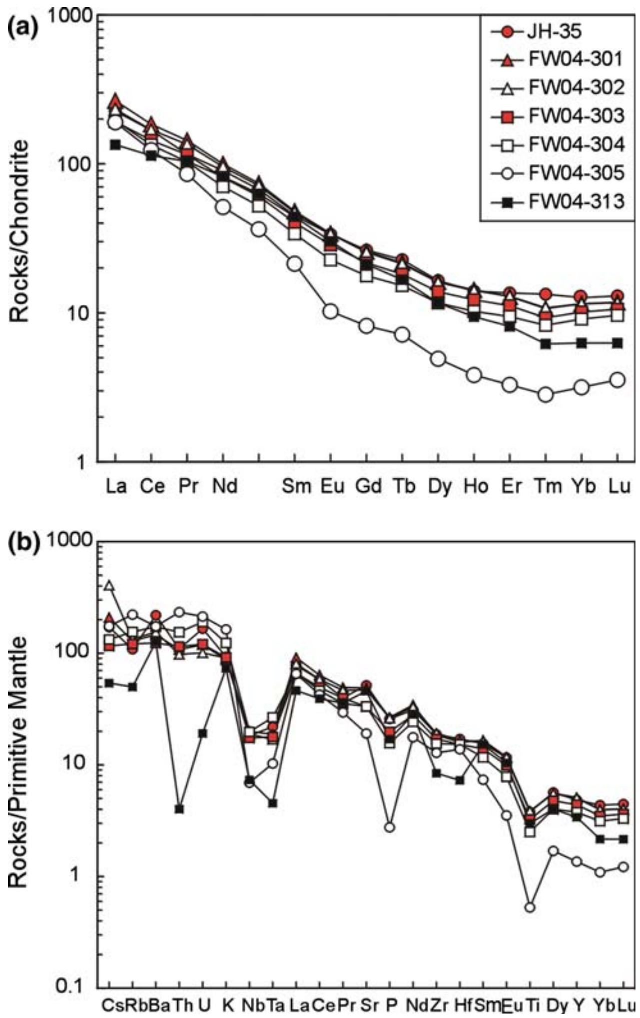


**Fig. 2** **a** Chondrite-normalized REE patterns and **b** primitive mantle (PM) normalized trace element patterns for monzogranite, enclaves and wall rock (Archean gneiss) of the Gudaoling batholith. Sample number refers to rocks analyzed in Table 1. Elements in **b** are arranged in the order of decreasing incompatibility from left to right. The Chondrite and PM values are from Sun and McDonough (1989)

U, Th and Pb concentrations were calibrated by using $^{29}$Si as the internal calibrant and NIST 610 as the reference material. The $^{207}$Pb/$^{206}$Pb and $^{206}$Pb/$^{238}$U ratios were calculated using the GLITTER program, which were then corrected using the Harvard zircon 91500 as external calibrant. According to the method of Ballard et al. (2001), measured $^{207}$Pb/$^{206}$Pb, $^{206}$Pb/$^{238}$U and $^{208}$Pb/$^{232}$Th ratios in zircon 91500 were averaged over the course of the analytical session and used to calculate correction factors. These correction factors were then applied to each sample to correct for both instrumental mass bias and depth-dependent elemental and isotopic fractionation. The detailed analytical technique is described in Yuan et al. (2004). The $^{204}$Pb isotope cannot be precisely measured with this technique, due to a combination of low signal and interference from small amounts of $^{204}$Hg in the Ar gas supply. We used the $^{208}$Pb/$^{206}$Pb–$^{232}$Th/$^{238}$U ratios to see if there was any significant disturbance for the enclaves, monzogranite and Archean gneiss (unshown), but no significant disturbance was detected. Common Pb contents were therefore evaluated using the method described by Andersen (2002). The age calculations and plotting of concordia diagrams were made using ISOPLOT (ver 3.0) (Ludwig 2003). The errors quoted in tables and figures are at the 2$\sigma$ levels.

In situ zircon Hf isotopic analyses were conducted using a Neptune MC-ICPMS, equipped with a 193 nm laser, at the Institute of Geology and Geophysics, Chinese Academy of Sciences in Beijing, China. During analyses, a laser repetition rate of 10 Hz at 100 mJ was used and spot sizes were either 32 or 63 μm. Raw count rates for $^{172}$Yb, $^{173}$Yb, $^{175}$Lu, $^{176}$(Hf + Yb + Lu), $^{177}$Hf, $^{178}$Hf, $^{179}$Hf, $^{180}$Hf and $^{182}$W were collected and isobaric interference corrections for $^{176}$Lu and $^{176}$Yb on $^{176}$Hf must be determined precisely. $^{176}$Lu was calibrated using the $^{175}$Lu value and the correction was made to $^{176}$Hf. The $^{176}$Yb/$^{172}$Yb value of 0.5887 and mean $\beta_{Yb}$ value obtained during Hf analysis on the same spot were applied for the interference correction of $^{176}$Yb on $^{176}$Hf (Iizuka and Hirata 2005). The detailed analytical technique is described in Wu et al. (2006). During analyses, the $^{176}$Hf/$^{177}$Hf and $^{176}$Lu/$^{177}$Hf ratios of the standard zircon (91500) were 0.282294 ± 15 ($2\sigma_n$, $n = 20$) and 0.00031, similar to the commonly accepted $^{176}$Hf/$^{177}$Hf ratio of 0.282302 ± 8 and 0.282306 ± 8 (2$\sigma$) measured using the solution method (Goolaerts et al. 2004; Woodhead et al. 2004). The notations of $\varepsilon_{Hf}$, $f_{Lu/Hf}$, $T_{DM}$ and $T_{DM}^{C}$ are defined as in Yang et al. (2006b).

## Analytical results

A total of 117 zircon grains from seven samples, including mafic microgranular enclaves, host granite and Archean gneissic wall rock, were selected for study. The zircon CL images, U–Pb and Hf isotopic results are presented in Figs. 3, 4, 5, 6 and the data are listed in Electronic Supplementary Material (ESM) and shortened in Table 2.

### Zircon CL images and U–Pb data

Zircons from gneiss sample FW04–313, host rock of the Gudaoling batholith, are round to ovoid or prismatic,

**Table 1** Major and trace elements of Gudaoling monzgranite, mafic enclaves and wall-rock gneiss

| Sample no. | JH-35 | FW04-301 | FW04-302 | FW04-303 | FW04-304 | FW04-305 | FW04-313 |
|---|---|---|---|---|---|---|---|
| Rock type | Mafic enclave | | | | | Monzogranite | Gneiss |
| *Major elements (wt%)* | | | | | | | |
| $SiO_2$ | 53.66 | 53.70 | 53.42 | 57.60 | 62.99 | 73.03 | 58.11 |
| $TiO_2$ | 0.86 | 0.87 | 0.88 | 0.74 | 0.57 | 0.12 | 0.68 |
| $Al_2O_3$ | 15.92 | 15.53 | 15.32 | 14.42 | 14.95 | 14.09 | 16.84 |
| $Fe_2O_{3T}$ | 6.27 | 6.91 | 7.04 | 6.06 | 4.38 | 1.50 | 7.45 |
| MnO | 0.10 | 0.11 | 0.12 | 0.12 | 0.07 | 0.02 | 0.09 |
| MgO | 6.21 | 6.86 | 7.36 | 6.14 | 3.61 | 0.31 | 3.39 |
| CaO | 7.63 | 7.63 | 7.73 | 6.78 | 4.51 | 1.21 | 5.55 |
| $Na_2O$ | 3.82 | 3.86 | 3.54 | 3.83 | 3.86 | 3.93 | 4.61 |
| $K_2O$ | 2.80 | 2.63 | 2.73 | 2.76 | 3.72 | 4.92 | 2.21 |
| $P_2O_5$ | 0.56 | 0.58 | 0.57 | 0.43 | 0.34 | 0.06 | 0.37 |
| LOI | | 0.85 | 0.82 | 0.64 | 0.58 | 0.44 | 0.52 |
| Total | 97.82 | 99.53 | 99.53 | 99.52 | 99.58 | 99.63 | 99.82 |
| Mg# | 66.5 | 66.5 | 67.6 | 67.0 | 62.2 | 29.2 | 47.6 |
| *Trace elements (ppm)* | | | | | | | |
| V | 115 | 135 | 140 | 122 | 85.3 | 12.8 | 129 |
| Cr | 161 | 196 | 222 | 193 | 99.9 | 4.18 | 37.6 |
| Ni | 107 | 109 | 125 | 91.7 | 50.5 | 3.05 | 24.8 |
| Ga | 16.9 | 16.7 | 16.4 | 16.3 | 16.6 | 16.9 | 21.8 |
| Rb | 68.9 | 81.7 | 85.3 | 77.1 | 98.7 | 141 | 31.7 |
| Sr | 1,088 | 1,032 | 990 | 701 | 705 | 403 | 968 |
| Y | 22.1 | 23.2 | 23.0 | 20.0 | 17.1 | 6.18 | 15.4 |
| Zr | 210 | 207 | 215 | 191 | 174 | 144 | 94.3 |
| Nb | 13.0 | 14.2 | 13.5 | 12.4 | 14.1 | 4.94 | 5.23 |
| Cs | 1.35 | 1.65 | 3.21 | 0.92 | 1.05 | 1.38 | 0.43 |
| Ba | 1,532 | 1,025 | 1,080 | 865 | 1,206 | 1,216 | 883 |
| La | 53.6 | 62.7 | 55.2 | 45.5 | 46.1 | 45.0 | 31.9 |
| Ce | 103 | 113 | 104 | 87.9 | 82.0 | 75.6 | 69.5 |
| Pr | 11 | 13.6 | 12.8 | 10.9 | 9.79 | 8.13 | 9.87 |
| Nd | 42.1 | 46.6 | 44.7 | 37.8 | 32.9 | 24.0 | 38.3 |
| Sm | 6.87 | 7.36 | 7.19 | 6.18 | 5.19 | 3.27 | 6.76 |
| Eu | 1.95 | 1.98 | 1.96 | 1.66 | 1.32 | 0.59 | 1.75 |
| Gd | 5.93 | 5.94 | 5.88 | 5.05 | 4.23 | 2.36 | 4.97 |
| Tb | 0.85 | 0.81 | 0.80 | 0.68 | 0.57 | 0.27 | 0.63 |
| Dy | 4.18 | 4.09 | 4.07 | 3.52 | 2.96 | 1.25 | 2.96 |
| Ho | 0.79 | 0.81 | 0.80 | 0.69 | 0.58 | 0.22 | 0.53 |
| Er | 2.25 | 2.13 | 2.14 | 1.85 | 1.56 | 0.54 | 1.34 |
| Tm | 0.34 | 0.27 | 0.28 | 0.24 | 0.21 | 0.07 | 0.16 |
| Yb | 2.15 | 1.96 | 1.95 | 1.72 | 1.54 | 0.54 | 1.07 |
| Lu | 0.33 | 0.30 | 0.30 | 0.27 | 0.24 | 0.09 | 0.16 |
| Hf | 5.27 | 4.93 | 5.11 | 4.70 | 4.72 | 4.27 | 2.25 |
| Ta | 0.90 | 0.77 | 0.69 | 0.73 | 1.09 | 0.42 | 0.19 |
| Pb | 9.50 | 7.88 | 6.61 | 10.6 | 9.98 | 22.7 | 8.73 |
| Th | 9.30 | 9.18 | 8.32 | 9.75 | 13.2 | 19.9 | 0.34 |
| U | 3.48 | 2.51 | 2.12 | 12.5 | 4.00 | 4.47 | 0.40 |

and many have weak oscillatory zones (Fig. 3a). Nineteen analyses form a coherent group with a weighted mean $^{207}Pb/^{206}Pb$ age of 2518 ± 7 Ma (Fig. 4a), which is interpreted to represent the formation age of its protolith.

CL images and U–Pb data show that two groups of zircons are present in monzogranite sample FW04-305: (1) rare round to ovoid and prismatic grains that show weak oscillatory zones (Fig. 3b), similar to those in the host gneiss. These have $^{207}Pb/^{206}Pb$ ages ranging from 2,522 ± 55 to 1,935 ± 41 Ma (Figs. 3b, 4b); and (2) prismatic grains that either have oscillatory zones or light cores with oscillatory-zoned rims (Fig. 3b) in CL image. Among the 25 U–Pb analyses of these grains, two have $^{206}Pb/^{238}U$ ages of 163 ± 2 and 157 ± 2 Ma (Fig. 4b). The remaining 16 analyses are younger and form a coherent group with a weighted mean $^{206}Pb/^{238}U$ age of 120 ± 1 Ma (Figs. 3b, 4b), which is taken to represent the time of magmatic crystallization.

Zircons from the enclave samples (FW04-301, 302, 303, 304 and JH-35) fall into four groups based on their CL patterns and U–Pb ages: (1) rounded ovoid and prismatic grains in samples FW04-302, 303 and 304 have weak oscillatory zones (Fig. 3c) and $^{207}Pb/^{206}Pb$

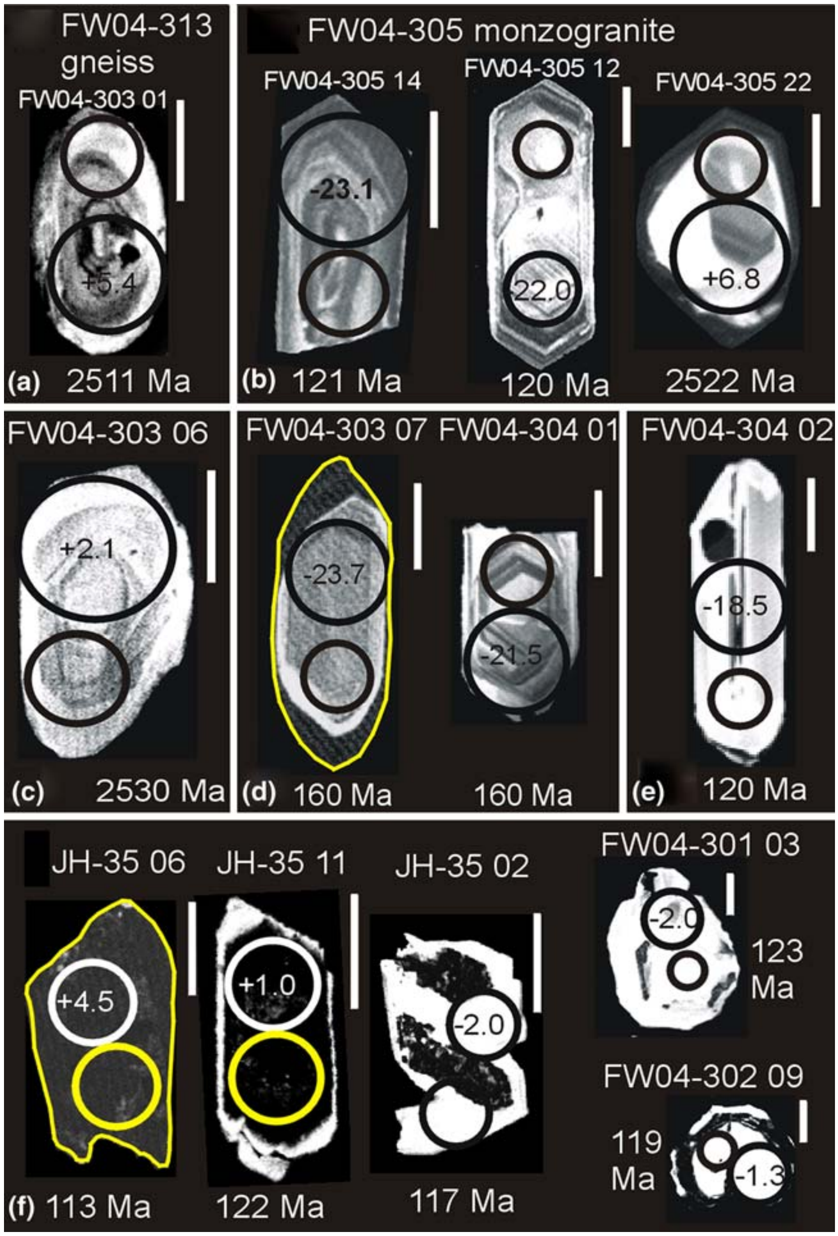


**Fig. 3** Cathodoluminescence (CL) images of representative zircons from **a** Archean gneiss, **b** Gudaoling monzogranite and **c–f** microdiorite enclaves. *Circles with enclosed data* indicate the location of LA-MC-ICPMS Hf analyses and the enclosed data refer to the $\varepsilon_{Hf}(t)$ values, whereas *circles without data* indicate the location of LA-ICPMS U–Pb analyses. U–Pb ages are listed under individual zircons and spot numbers presented above the zircon images are the sample number as listed in Table 2. All $\varepsilon_{Hf}(t)$ values were calculated at the age of individual zircons. The scale bar is 50 μm

ages of 2,530–2,376 Ma (Fig. 4c) are interpreted as inherited grains; (2) prismatic grains in samples FW04-303 and 304 have oscillatory zones or are homogeneous and light in CL images (Fig. 3d). Two analyses of two grains give a $^{206}Pb/^{238}U$ age of 160 ± 1 Ma (Fig. 4c); (3) prismatic grains in samples FW04-303 and 304 have oscillatory zones or are homogeneous and light in CL images, similar to those from the host granites (Fig. 3e). Four analyses of four grains form a coherent group with a weighted mean $^{206}Pb/^{238}U$ age of 118 ± 2 Ma (Fig. 4c) and (4) the main group of zircons in all enclaves are anhedral, elongate grains that have relatively dark, homogeneous CL images or have dark cores and lighter rims that are separated by irregular interfaces indicative of corrosion (Fig. 3f). Oscillatory zoning is absent within these crystals. Fifty-two analyses of 52 grains form a coherent group with a weighted mean $^{206}Pb/^{238}U$ age of 120 ± 1 Ma (Fig. 4c).

## Zircon Hf isotopic compositions

Zircons from gneiss sample FW04-313 have variable Hf isotopic compositions with $^{176}Hf/^{177}Hf$ ratios from 0.281222 to 0.281401 and $\varepsilon_{Hf}(t)$ values from +0.1 to +7.6 ($t$ = 2,516 Ma) (Table 2).

The main group of zircons from monzogranite sample FW04-305 with a $^{206}Pb/^{238}U$ age of ~120 Ma have initial $^{176}Hf/^{177}Hf$ ratios of 0.281980–0.282271 and

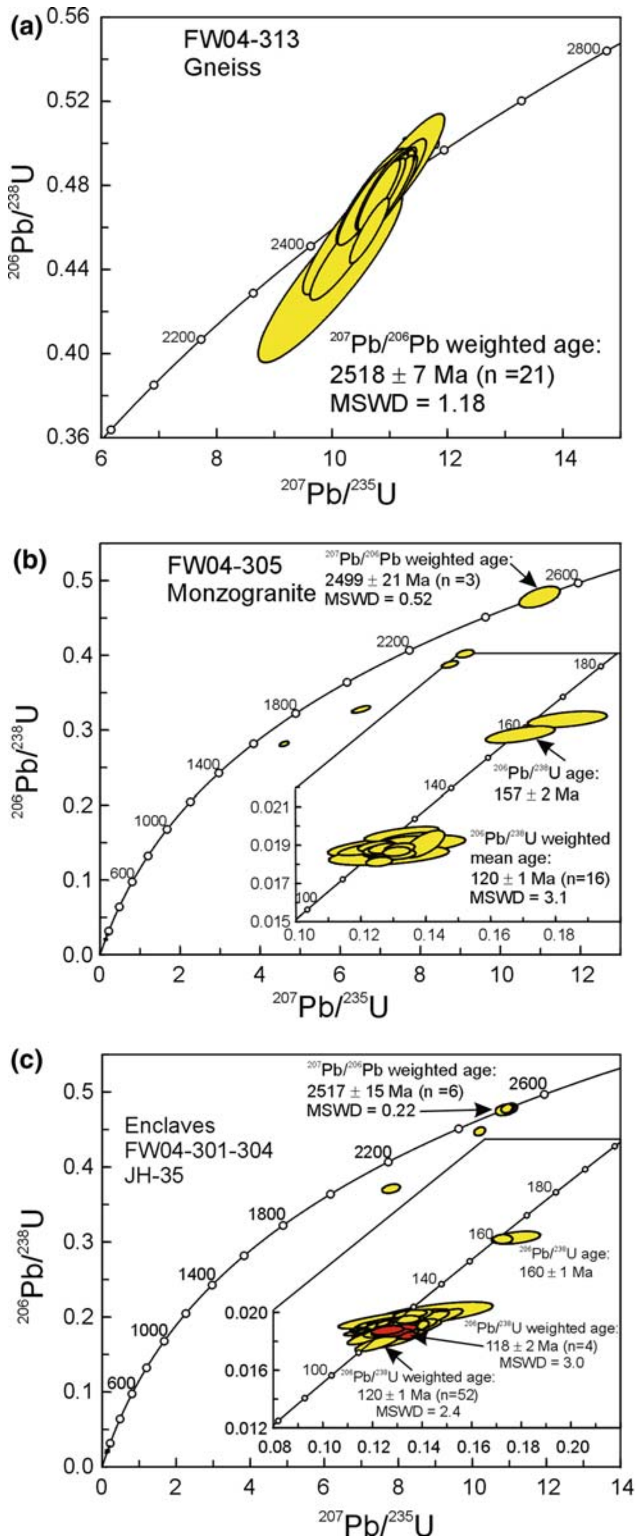


**Fig. 4** LA-ICPMS U–Pb zircon concordia diagrams for **a** Archean gneiss (FW04-313), **b** monzogranite (FW04-305) and **c** mafic enclaves (FW04-301–304 and JH-35) from the Gudaoling batholith, Liaodong Peninsula, NE China. Ellipse dimensions are 2$\sigma$

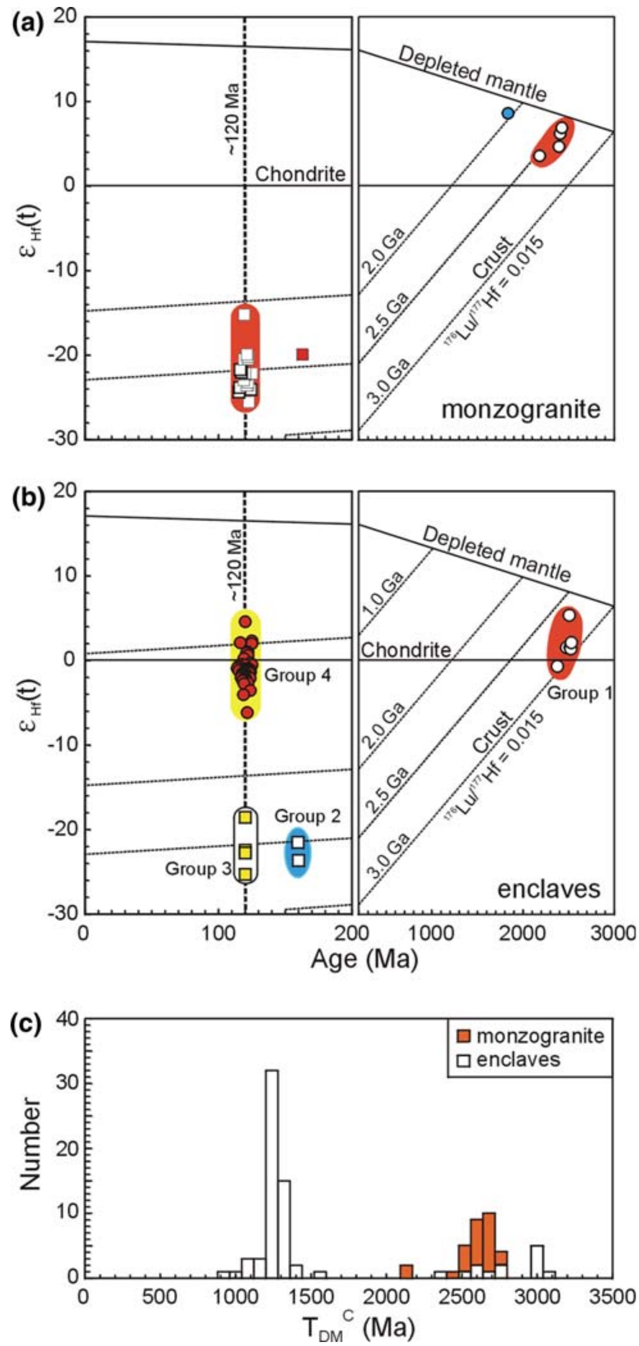


**Fig. 5** Zircon Hf isotopic compositions of **a** monzogranite (FW04-305) and **b** mafic enclaves (FW04-301–304 and JH-35) from the Gudaoling batholith, Liaodong Peninsula, NE China. The $\varepsilon_{Hf}(t)$ of each zircon was calculated at its U–Pb age. **c** Histogram of $T_{DM}^{C}$ values of zircons from enclaves and host monzogranite

$\varepsilon_{Hf}(t)$ values of –15.1 to –25.4 (Fig. 5a). However, the Jurassic zircons (~160 Ma) have initial $^{176}Hf/^{177}Hf$ ratios of 0.282036–0.282111 and the Precambrian zircons have initial $^{176}Hf/^{177}Hf$ ratios between 0.281322

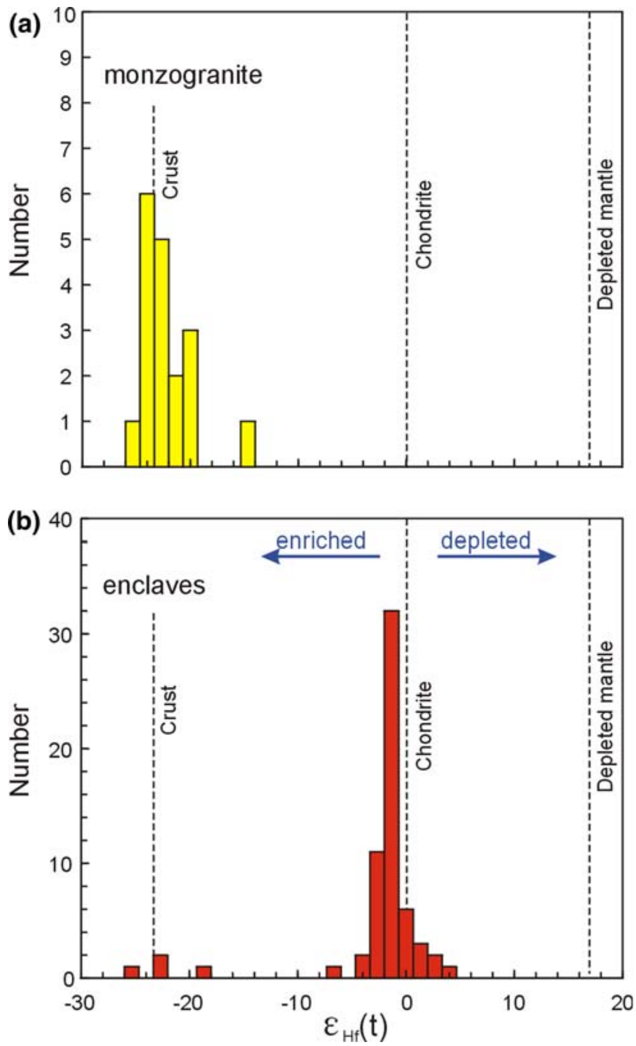


**Fig. 6** Histograms of $\varepsilon_{Hf}(t)$ values of zircons with an age of 120 Ma in **a** monzogranite (FW04-305) and **b** mafic enclaves (FW04-301–304 and JH-35) from the Gudaoling batholith, Liaodong Peninsula, NE China. $\varepsilon_{Hf}(t)$ values of all zircons were calculated at 120 Ma, the crystallization age of mafic enclaves and host granite

and 0.281791, corresponding to $\varepsilon_{Hf}(t)$ values between +3.5 to +8.5 (Table 2; Figs. 3b, 5a).

The main group of zircons (Group 4) from the enclave samples (FW04-301–304 and JH-35) with a $^{206}Pb/^{238}U$ age of ~120 Ma (Fig. 4c) show a large range of initial $^{176}Hf/^{177}Hf$ ratios from 0.282521 to 0.282929 with $\varepsilon_{Hf}(t)$ values from –6.2 ± 0.7 to +4.5 ± 0.9 (Table 2; Fig. 5b). The prismatic grains (Group 3) in enclave samples FW04-303 and 304, having CL images and U–Pb ages similar to those from the host granites (Fig. 3e), have initial $^{176}Hf/^{177}Hf$ ratios of 0.281983–0.282173 and $\varepsilon_{Hf}(t)$ values of –25.3 to –18.5 (Table 2; Fig. 5b). The Jurassic (~160 Ma) zircons (Group 2) in enclave samples FW04-303 and 304 have $\varepsilon_{Hf}(t)$ values of –23.7 to –21.5. The Precambrian zircons (Group 1) in enclave samples FW04-302, 303 and 304 have initial $^{176}Hf/^{177}Hf$ ratios ranging from 0.281211 to 0.281334 [$\varepsilon_{Hf}(t)$ = –0.7 to +5.3) (Table 2; Fig. 5b).

## Discussion

### Age of the Gudaoling Batholith

The Gudaoling monzogranite contains inherited zircons yielding ages in the ranges 2,530–2,477, 2,280–1,935 and ~160 Ma (Fig. 4b), whereas, the enclaves contain inherited zircons with ages of 2,523–2,376 Ma and ~160 Ma (Fig. 4c). The dominance of the 2,530–2,477 Ma age group in the inherited populations can be related to the emplacement age and time of high-grade metamorphism of the basement rocks in the Liaodong Peninsula (Zhao et al. 2001; Luo et al. 2004; Lu et al. 2004), whereas, the ages of 2.3–1.9 Ga and ~160 Ma are consistent with the emplacement ages of Proterozoic and Jurassic granitic intrusions, respectively (Lu et al. 2004; Wu et al. 2005b). Therefore, these older zircons are considered to be inherited from the source region or introduced by contamination during magma ascent through the crust.

The magmatic zircons from the Gudaoling monzogranite and microgranular enclaves both have ages of 120 ± 1 Ma (Fig. 4b, c), which means that the time of crystallization of the monzogranite and its enclaves was identical. These ages agree with previous zircon U–Pb ages of 118 ± 3 and 122 ± 2 Ma published for the Gudaoling batholith (Yang et al. 2004a). Therefore, they establish that the mafic and felsic magmas were indeed coeval.

### Causes of Hf isotopic variation and origin of the enclaves

The wide range of Hf isotopic compositions from the Gudaoling batholith precludes a simple, common evolution by closed-system fractionation processes, since this mechanism cannot produce the observed changes over the time scales allowed by the age of the batholith. Other mechanisms, such as restite separation, wall-rock assimilation or magma mixing may potentially explain this.

Three enclave samples (FW04-302, 303 and 304) contain varying proportions of inherited zircons (Table 2). The presence of inherited zircons in enclaves has previously been used to infer a restitic origin (Chappell et al. 1987; Chappell and Stephens

**Table 2** U–Pb ages (Ma) and Hf isotopic data of zircons from the enclaves, host granite and wall-rock of the Gudaoling Batholith, Liaodong Peninsula, NE China

| Spots | U–Pb ages (Ma) | | | | | | Hf isotopes | | | | |
|---|---|---|---|---|---|---|---|---|---|---|---|
| | $^{206}Pb/^{238}U$ | ±2σ | $^{207}Pb/^{235}U$ | ±2σ | $^{207}Pb/^{206}Pb$ | ±2σ | $^{176}Hf/^{177}Hf$ | ±2σ | $\varepsilon_{Hf}(t)$* | $T_{DM}$* (Ma) | $T^{C}_{DM}$* (Ma) |
| *FW04-313 gneiss, wall rock* | | | | | | | | | | | |
| 01 | 2,517 | 61 | 2,518 | 27 | 2,518 | 22 | 0.281232 | 0.000013 | 1.1 | 2,787 | 3,054 |
| 02 | 2,489 | 72 | 2,488 | 36 | 2,488 | 29 | 0.281407 | 0.000015 | 6.8 | 2,533 | 2,654 |
| 03 | 2,510 | 60 | 2,514 | 26 | 2,517 | 22 | 0.281260 | 0.000014 | 1.3 | 2,756 | 3,019 |
| 04 | 2,514 | 64 | 2,513 | 29 | 2,513 | 24 | 0.281222 | 0.000012 | 0.1 | 2,826 | 3,117 |
| 05 | 2,497 | 85 | 2,508 | 44 | 2,518 | 36 | 0.281234 | 0.000014 | 1.0 | 2,782 | 3,052 |
| 06 | 2,504 | 71 | 2,521 | 34 | 2,535 | 28 | 0.281222 | 0.000013 | 0.7 | 2,793 | 3,072 |
| 07 | 2,545 | 105 | 2,532 | 57 | 2,522 | 46 | 0.281242 | 0.000013 | 2.0 | 2,769 | 3,012 |
| 08 | 2,384 | 82 | 2,455 | 45 | 2,515 | 37 | 0.281268 | 0.000011 | 2.7 | 2,737 | 2,961 |
| 09 | 2,526 | 79 | 2,527 | 40 | 2,528 | 32 | 0.281306 | 0.000014 | 4.0 | 2,696 | 2,886 |
| 10 | 2,523 | 63 | 2,524 | 28 | 2,526 | 23 | 0.281254 | 0.000010 | 1.8 | 2,755 | 3,005 |
| 11 | 2,528 | 63 | 2,527 | 28 | 2,526 | 23 | 0.281320 | 0.000013 | 4.4 | 2,663 | 2,845 |
| 12 | 2,502 | 82 | 2,495 | 43 | 2,489 | 35 | 0.281249 | 0.000013 | 1.8 | 2,762 | 3,012 |
| 13 | 2,520 | 62 | 2,516 | 28 | 2,513 | 23 | 0.281255 | 0.000012 | 1.9 | 2,737 | 2,987 |
| 14 | 2,520 | 66 | 2,512 | 31 | 2,505 | 25 | 0.281208 | 0.000010 | 0.4 | 2,804 | 3,091 |
| 15 | 2,423 | 103 | 2,461 | 59 | 2,493 | 49 | 0.281227 | 0.000014 | 0.7 | 2,789 | 3,067 |
| 16 | 2,509 | 75 | 2,506 | 37 | 2,503 | 30 | 0.281242 | 0.000013 | 1.0 | 2,768 | 3,039 |
| 17 | 2,431 | 56 | 2,493 | 24 | 2,543 | 21 | 0.281401 | 0.000017 | 7.6 | 2,556 | 2,653 |
| 18 | 2,514 | 60 | 2,526 | 26 | 2,535 | 22 | 0.281231 | 0.000012 | 1.1 | 2,790 | 3,056 |
| 19 | 2,518 | 70 | 2,513 | 33 | 2,509 | 27 | 0.281258 | 0.000013 | 1.2 | 2,761 | 3,027 |
| 20 | 2,335 | 151 | 2,431 | 94 | 2,513 | 81 | | | | | |
| 21 | 2,506 | 59 | 2,507 | 26 | 2,507 | 22 | | | | | |
| *FW04-305 monzogranite* | | | | | | | | | | | |
| 01 | 118 | 2 | 126 | 7 | 270 | 118 | 0.281983 | 0.000012 | –25.4 | 1,806 | 2,768 |
| 02 | 120 | 1 | 121 | 4 | 142 | 77 | 0.282123 | 0.000011 | –20.4 | 1,588 | 2,458 |
| 03 | 119 | 1 | 125 | 3 | 241 | 61 | 0.282082 | 0.000011 | –21.9 | 1,667 | 2,550 |
| 04 | 121 | 2 | 125 | 8 | 210 | 132 | 0.282076 | 0.000009 | –22.1 | 1,663 | 2,561 |
| 05 | 120 | 1 | 122 | 4 | 156 | 72 | 0.282025 | 0.000010 | –24.0 | 1,773 | 2,678 |
| 06 | 118 | 3 | 123 | 14 | 224 | 219 | 0.282033 | 0.000009 | –23.6 | 1,696 | 2,655 |
| 07 | 119 | 2 | 124 | 6 | 203 | 110 | 0.282132 | 0.000018 | –20.1 | 1,568 | 2,438 |
| 08 | 1,822 | 19 | 2,046 | 26 | 2,280 | 57 | 0.281441 | 0.000014 | 3.5 | 2,488 | 2,701 |
| 09 | 118 | 1 | 126 | 3 | 280 | 64 | 0.282039 | 0.000010 | –23.4 | 1,717 | 2,645 |
| 10 | 121 | 3 | 125 | 16 | 207 | 242 | 0.282273 | 0.000012 | –15.1 | 1,389 | 2,128 |
| 11 | 2,109 | 18 | 2,309 | 18 | 2,491 | 29 | 0.281369 | 0.000011 | 4.6 | 2,631 | 2,807 |
| 12 | 122 | 4 | 133 | 5 | 335 | 67 | 0.282077 | 0.000016 | –22.0 | 1,659 | 2,560 |
| 13 | 157 | 2 | 159 | 8 | 175 | 103 | 0.282053 | 0.000014 | –22.0 | 1,656 | 2,587 |
| 14 | 121 | 2 | 127 | 7 | 244 | 111 | 0.282050 | 0.000022 | –23.1 | 1,758 | 2,625 |
| 15 | 163 | 2 | 171 | 9 | 291 | 131 | 0.282114 | 0.000015 | –19.8 | 1,595 | 2,455 |
| 16 | 2,176 | 20 | 2,349 | 18 | 2,503 | 39 | 0.281388 | 0.000017 | 6.1 | 2,582 | 2,720 |
| 17 | 121 | 1 | 119 | 4 | 91 | 77 | 0.282125 | 0.000012 | –20.3 | 1,591 | 2,455 |
| 18 | 116 | 1 | 120 | 3 | 211 | 61 | 0.282093 | 0.000009 | –21.6 | 1,644 | 2,528 |
| 19 | 122 | 2 | 126 | 6 | 199 | 104 | 0.282025 | 0.000012 | –23.8 | 1,715 | 2,672 |
| 20 | 123 | 2 | 128 | 7 | 219 | 111 | 0.282074 | 0.000012 | –22.1 | 1,659 | 2,564 |
| 21 | 125 | 2 | 126 | 8 | 156 | 134 | 0.282014 | 0.000014 | –24.2 | 1,782 | 2,699 |
| 22 | 2,517 | 50 | 2,520 | 35 | 2,522 | 55 | 0.281399 | 0.000013 | 6.8 | 2,572 | 2,691 |
| 23 | 120 | 2 | 118 | 8 | 82 | 132 | 0.282055 | 0.000011 | –22.8 | 1,684 | 2,608 |
| 24 | 120 | 1 | 126 | 3 | 236 | 65 | 0.282038 | 0.000015 | –23.5 | 1,746 | 2,649 |
| 25 | 1,593 | 14 | 1,747 | 17 | 1,935 | 41 | 0.281836 | 0.000016 | 8.5 | 2,002 | 2,094 |
| *FW04-301 enclave* | | | | | | | | | | | |
| 01 | 123 | 2 | 123 | 5 | 125 | 105 | 0.282663 | 0.000015 | –1.2 | 821 | 1,257 |
| 02 | 121 | 2 | 120 | 9 | 112 | 187 | 0.282659 | 0.000013 | –1.4 | 828 | 1,267 |
| 03 | 123 | 2 | 126 | 6 | 178 | 131 | 0.282643 | 0.000013 | –2.0 | 883 | 1,308 |
| 04 | 118 | 2 | 126 | 5 | 266 | 113 | 0.282654 | 0.000010 | –1.6 | 836 | 1,280 |
| 05 | 121 | 2 | 123 | 6 | 155 | 121 | 0.282671 | 0.000011 | –1.0 | 812 | 1,240 |
| 06 | 120 | 2 | 119 | 7 | 102 | 156 | 0.282656 | 0.000010 | –1.5 | 831 | 1,273 |
| 07 | 123 | 2 | 120 | 6 | 75 | 122 | 0.282664 | 0.000011 | –1.2 | 821 | 1,254 |
| 08 | 124 | 2 | 126 | 6 | 174 | 128 | 0.282667 | 0.000010 | –1.1 | 833 | 1,251 |

**Table 2** continued

| Spots | U–Pb ages (Ma) | | | | | | Hf isotopes | | | | |
|---|---|---|---|---|---|---|---|---|---|---|---|
| | $^{206}Pb/^{238}U$ | $\pm 2\sigma$ | $^{207}Pb/^{235}U$ | $\pm 2\sigma$ | $^{207}Pb/^{206}Pb$ | $\pm 2\sigma$ | $^{176}Hf/^{177}Hf$ | $\pm 2\sigma$ | $\varepsilon_{Hf}(t)$* | $T_{DM}$* (Ma) | $T_{DM}^{C}$* (Ma) |
| 09 | 119 | 2 | 123 | 7 | 201 | 140 | 0.282662 | 0.000011 | –1.4 | 833 | 1,263 |
| 10 | 119 | 2 | 119 | 7 | 120 | 144 | 0.282650 | 0.000011 | –1.8 | 848 | 1,290 |
| 11 | 122 | 2 | 125 | 6 | 190 | 120 | 0.282662 | 0.000010 | –1.3 | 829 | 1,261 |
| 12 | 119 | 2 | 122 | 6 | 174 | 130 | 0.282639 | 0.000010 | –2.2 | 869 | 1,315 |
| 13 | 120 | 1 | 120 | 4 | 121 | 87 | 0.282640 | 0.000010 | –2.1 | 859 | 1,310 |
| 14 | 122 | 2 | 125 | 4 | 191 | 98 | 0.282656 | 0.000008 | –1.5 | 832 | 1,272 |
| 15 | 119 | 1 | 123 | 4 | 187 | 89 | 0.282664 | 0.000011 | –1.3 | 841 | 1,261 |
| 16 | 119 | 2 | 122 | 7 | 177 | 144 | 0.282633 | 0.000010 | –2.3 | 864 | 1,326 |
| 17 | 118 | 2 | 120 | 8 | 162 | 168 | 0.282658 | 0.000010 | –1.5 | 830 | 1,271 |
| 18 | 124 | 2 | 127 | 5 | 190 | 103 | 0.282642 | 0.000011 | –2.1 | 899 | 1,312 |
| 19 | 122 | 2 | 120 | 6 | 91 | 122 | 0.282644 | 0.000009 | –1.9 | 848 | 1,300 |
| 20 | 119 | 2 | 123 | 7 | 207 | 138 | 0.282672 | 0.000009 | –0.9 | 809 | 1,238 |
| 21 | 121 | 2 | 123 | 6 | 166 | 132 | 0.282666 | 0.000012 | –1.2 | 821 | 1,252 |
| *FW04-302 enclave* | | | | | | | | | | | |
| 01 | 120 | 2 | 120 | 9 | 118 | 196 | 0.282669 | 0.000012 | –1.1 | 816 | 1,246 |
| 02 | 122 | 3 | 122 | 13 | 135 | 246 | 0.282671 | 0.000013 | –1.0 | 817 | 1,240 |
| 03 | 117 | 2 | 127 | 7 | 301 | 139 | 0.282689 | 0.000012 | –0.5 | 806 | 1,205 |
| 04 | 120 | 2 | 120 | 13 | 124 | 244 | 0.282647 | 0.000010 | –1.8 | 847 | 1,295 |
| 05 | 123 | 2 | 123 | 11 | 114 | 218 | 0.282662 | 0.000009 | –1.2 | 825 | 1,259 |
| 06 | 2,507 | 23 | 2,506 | 12 | 2,506 | 37 | 0.281349 | 0.000014 | 5.3 | 2,612 | 2,770 |
| 07 | 119 | 2 | 123 | 8 | 201 | 158 | 0.282670 | 0.000011 | –1.0 | 820 | 1,244 |
| 08 | 118 | 2 | 118 | 5 | 112 | 108 | 0.282659 | 0.000013 | –1.5 | 851 | 1,272 |
| 09 | 119 | 2 | 121 | 11 | 173 | 220 | 0.282663 | 0.000011 | –1.3 | 825 | 1,258 |
| 10 | 118 | 2 | 121 | 11 | 180 | 217 | 0.282668 | 0.000010 | –1.1 | 816 | 1,247 |
| 11 | 117 | 2 | 122 | 7 | 207 | 142 | 0.282664 | 0.000015 | –1.3 | 822 | 1,257 |
| 12 | 119 | 3 | 123 | 12 | 202 | 240 | 0.282637 | 0.000013 | –2.2 | 858 | 1,317 |
| 13 | 123 | 2 | 121 | 10 | 87 | 193 | 0.282655 | 0.000011 | –1.5 | 833 | 1,274 |
| 14 | 122 | 2 | 125 | 11 | 173 | 211 | 0.282670 | 0.000010 | –1.0 | 812 | 1,240 |
| 15 | 124 | 4 | 123 | 17 | 104 | 285 | 0.282658 | 0.000011 | –1.3 | 830 | 1,266 |
| *FW04-303 enclave* | | | | | | | | | | | |
| 01 | 119 | 1 | 119 | 2 | 114 | 60 | 0.282624 | 0.000013 | –2.8 | 903 | 1,352 |
| 02 | 119 | 1 | 123 | 4 | 209 | 97 | 0.282643 | 0.000017 | –2.2 | 918 | 1,318 |
| 03 | 2,519 | 22 | 2,518 | 11 | 2,517 | 36 | 0.281239 | 0.000015 | 1.6 | 2,764 | 3,020 |
| 04 | 2,384 | 21 | 2,453 | 11 | 2,510 | 36 | 0.281272 | 0.000015 | 1.5 | 2,732 | 2,989 |
| 05 | 2,513 | 25 | 2,514 | 14 | 2,515 | 39 | 0.281266 | 0.000017 | 1.6 | 2,766 | 3,019 |
| 06 | 2,523 | 23 | 2,527 | 12 | 2,530 | 37 | 0.281271 | 0.000018 | 2.1 | 2,758 | 2,997 |
| 07 | 160 | 2 | 166 | 7 | 256 | 115 | 0.282006 | 0.000014 | –23.7 | 1,739 | 2,691 |
| 08 | 119 | 2 | 121 | 5 | 155 | 106 | 0.282589 | 0.000017 | –4.0 | 969 | 1,433 |
| 09 | 2,522 | 22 | 2,522 | 11 | 2,523 | 36 | 0.281240 | 0.000013 | 1.4 | 2,778 | 3,037 |
| 10 | 118 | 1 | 125 | 2 | 256 | 60 | 0.282634 | 0.000017 | –2.4 | 883 | 1,329 |
| 11 | 118 | 2 | 124 | 7 | 241 | 150 | 0.282652 | 0.000015 | –1.8 | 865 | 1,290 |
| 12 | 2,033 | 22 | 2,209 | 23 | 2,376 | 49 | 0.281276 | 0.000014 | –0.7 | 2,730 | 3,047 |
| 13 | 127 | 2 | 129 | 5 | 171 | 172 | 0.282599 | 0.000013 | –3.4 | 926 | 1,401 |
| *FW04-304 enclave* | | | | | | | | | | | |
| 01 | 160 | 2 | 162 | 3 | 194 | 129 | 0.282067 | 0.000013 | –21.5 | 1,657 | 2,558 |
| 02 | 120 | 2 | 124 | 6 | 213 | 60 | 0.282175 | 0.000013 | –18.5 | 1,513 | 2,343 |
| 03 | 118 | 1 | 123 | 5 | 220 | 123 | 0.282057 | 0.000013 | –22.8 | 1,671 | 2,603 |
| 04 | 117 | 1 | 128 | 3 | 342 | 119 | 0.282069 | 0.000014 | –22.4 | 1,690 | 2,582 |
| 05 | 119 | 2 | 121 | 5 | 145 | 161 | 0.281984 | 0.000014 | –25.3 | 1,761 | 2,761 |
| 06 | 124 | 1 | 128 | 4 | 194 | 108 | 0.282525 | 0.000019 | –6.2 | 1,048 | 1,571 |
| *JH-35 enclave* | | | | | | | | | | | |
| 01 | 121 | 3 | 130 | 7 | 304 | 100 | 0.282726 | 0.000015 | 0.9 | 759 | 1,121 |
| 02 | 117 | 3 | 114 | 6 | 66 | 93 | 0.282647 | 0.000014 | –2.0 | 885 | 1,304 |
| 03 | 109 | 3 | 111 | 7 | 156 | 108 | 0.282670 | 0.000015 | –1.3 | 826 | 1,252 |
| 04 | 115 | 3 | 153 | 8 | 798 | 89 | 0.282679 | 0.000021 | –0.9 | 828 | 1,231 |
| 05 | 122 | 3 | 122 | 7 | 115 | 100 | 0.282626 | 0.000031 | –2.7 | 921 | 1,349 |
| 06 | 113 | 3 | 117 | 6 | 205 | 98 | 0.282838 | 0.000027 | 4.5 | 641 | 887 |
| 07 | 122 | 3 | 121 | 7 | 98 | 96 | 0.282722 | 0.000027 | 0.6 | 811 | 1,141 |
| 08 | 120 | 3 | 127 | 7 | 269 | 97 | 0.282710 | 0.000020 | 0.2 | 803 | 1,163 |

**Table 2** continued

| Spots | U–Pb ages (Ma) | | | | | | Hf isotopes | | | | |
|---|---|---|---|---|---|---|---|---|---|---|---|
| | $^{206}Pb/^{238}U$ | $\pm 2\sigma$ | $^{207}Pb/^{235}U$ | $\pm 2\sigma$ | $^{207}Pb/^{206}Pb$ | $\pm 2\sigma$ | $^{176}Hf/^{177}Hf$ | $\pm 2\sigma$ | $\varepsilon_{Hf}(t)$* | $T_{DM}$* (Ma) | $T_{DM}^{C}$* (Ma) |
| 09 | 107 | 3 | 103 | 9 | 146 | 198 | 0.282773 | 0.000022 | 1.9 | 808 | 1,048 |
| 10 | 125 | 3 | 128 | 7 | 204 | 96 | 0.282773 | 0.000019 | 2.3 | 771 | 1,035 |
| 11 | 122 | 3 | 118 | 8 | 40 | 113 | 0.282742 | 0.000019 | 1.0 | 884 | 1,117 |
| 12 | 120 | 3 | 131 | 7 | 342 | 94 | 0.282684 | 0.000012 | –0.5 | 799 | 1,213 |
| 13 | 125 | 3 | 138 | 8 | 381 | 93 | 0.282684 | 0.000015 | –0.5 | 828 | 1,216 |
| 14 | 115 | 3 | 124 | 7 | 304 | 96 | 0.282688 | 0.000018 | –0.7 | 855 | 1,219 |
| 15 | 124 | 3 | 134 | 7 | 314 | 97 | 0.282695 | 0.000027 | –0.3 | 848 | 1,200 |
| 16 | 127 | 4 | 125 | 28 | 98 | 405 | 0.282763 | 0.000028 | 2.1 | 755 | 1,049 |

*$\varepsilon_{Hf(t)}$ = 10,000{[($^{176}Hf/^{177}Hf$)$_S$–($^{176}Lu/^{177}Hf$)$_S$ × ($e^{\lambda t}$–1)]/[($^{176}Hf/^{177}Hf$)$_{CHUR,0}$–($^{176}Lu/^{177}Hf$)$_{CHUR}$ × ($e^{\lambda t}$–1)]–1}

$T_{DM}$ = 1/$\lambda$ × ln{1 + [($^{176}Hf/^{177}Hf$)$_S$–($^{176}Hf/^{177}Hf$)$_{DM}$]/[($^{176}Lu/^{177}Hf$)$_S$–($^{176}Lu/^{177}Hf$)$_{DM}$]}

$T_{DM}^{C}$ = 1/$\lambda$ × ln{1 + [($^{176}Hf/^{177}Hf$)$_{S,t}$–($^{176}Hf/^{177}Hf$)$_{DM,t}$]/[($^{176}Lu/^{177}Hf$)$_C$–($^{176}Lu/^{177}Hf$)$_{DM}$]} + $t$

The $^{176}Hf/^{177}Hf$ and $^{176}Lu/^{177}Hf$ ratios of chondrite and depleted mantle at the present are 0.282772 and 0.0332, 0.28325 and 0.0384, respectively (Blichert-Toft and Albarède 1997; Griffin et al. 2000). $\lambda = 1.867 \times 10^{-11} a^{-1}$ (Soderlund et al. 2004). ($^{176}Lu/^{177}Hf$)$_C$ = 0.015, $t$ = crystallization age of zircon

1988; Chen et al. 1989; Chappell 1997; White et al. 1999; Chappell et al. 2000). If enclaves represent fragments of restite entrained from the source region of the magma, inheritance would be expected to be more pronounced in the enclaves than in the monzogranites. This does not hold for megacryst-poor enclaves (JH-35 and FW04-301), in which no inherited material was recognized. Moreover, in the restite model (Chappell et al. 1987; Chappell and Stephens 1988; Chen et al. 1989; Chappell 1997; White et al. 1999; Chappell et al. 2000), the mafic and felsic magmas would be expected to have similar isotopic compositions, which is not consistent with the observations from the Gudaoling batholith (Figs. 5, 6). Therefore, restite separation is unlikely to have produced the zircon Hf isotopic variations seen in the monzogranites and enclaves.

Reaction between magma and its wall rocks, provided that these are not the source rocks of the magma, could result in isotopic variations during crystallization of a magma. Some enclave and monzogranite samples have inherited zircons, potentially indicating wall-rock contamination. However, some enclaves (JH-35 and FW04-301) have no inherited zircons (Table 2). It is unlikely that the Lu–Hf isotopic systems of any inherited zircons within these enclaves have been reset, since this did not occur in the monzogranite (FW04-305) or the other enclaves (FW04-302, 303, and 304). Therefore, the absence of inherited zircons in samples JH-35 and FW04-301 suggests that this is not due to resetting, but due to very little reaction between the magma and its wall-rock.

Increasing recognition suggests that many magma chambers are open systems and may be fed with more primitive magma (which can be related or unrelated to magma already in the chamber) that caused a shift in the role assigned to microgranular enclaves (Eichelberger 1980; Vernon 1984; Holden et al. 1987; Vernon et al. 1988; Maas et al. 1997). Accordingly, enclaves may also be considered to represent remnants of a mafic component added to intermediate to felsic magma chambers. In the following discussion, we will argue that the isotopic and compositional variations in zircons from different rocks within the Gudaoling batholith are consistent with hybridization of magmas, as was originally suggested from the field characteristics, absence of cumulate textures in the enclave suite and from whole-rock compositional data (Yang et al. 2004a).

## Multiple sources for the Gudaoling Batholith

The monzogranites are peraluminous and have high $SiO_2$ and low MgO contents, initial $^{87}Sr/^{86}Sr$ ratios of 0.7055–0.7086 and strongly negative $\varepsilon_{Nd}(t)$ values (–18.5 to –20.9) (Yang et al. 2004a). A large proportion of the zircons in the granite are interpreted to have crystallized from the granitic magma, while some with less radiogenic Hf isotopes were inherited from the source rocks or were picked up from the wall rocks during magma emplacement. Magmatic zircons with an age of 120 Ma have strongly negative $\varepsilon_{Hf}(t)$ values (–15.1 to –25.4; Fig. 6a) and $T_{DM}^{C}$ ages of 2.8–2.1 Ga (most between 2.8 and 2.5 Ga, Table 2, Fig. 5c), suggesting that the parental magma was derived from a pre-existing crustal source that was separated from a depleted mantle source during the Late Archean. The large range of $\varepsilon_{Hf}(t)$ values of 120 Ma zircons suggests that the monzogranite was derived from an ancient crustal source with involvement of high $\varepsilon_{Hf}(t)$ materials.

The zircons from the enclave samples fall into four groups according to their CL patterns, U–Pb ages and Hf isotopic compositions. The grains of groups 1, 2 and 3 (Fig. 5b) could either have been introduced by mixing with the granitic magma or by assimilation of wall rocks. As most mafic microgranular enclaves contain megacrysts of feldspar and quartz, which are considered to have originated from the host granites, it is likely that these zircons have a similar origin (Barbarin 1990; Elburg 1996). This is also supported by these grains having similar appearance in CL images (Fig. 3) and similar Hf isotopic ratios to zircons from the host granites and the Archean gneiss wall rocks (Table 2).

The grains of group 4 from the enclaves, with an age of 120 Ma, have a large range of $\varepsilon_{Hf}(t)$ values from +4.5 to –6.2 (Figs. 5b, 6b). It is clear that a small proportion of group 4 zircons have positive $\varepsilon_{Hf}(t)$ values (up to +4.5) (Figs. 5b, 6b), indicating that they were derived from a source with time-integrated depletion [positive $\varepsilon_{Hf}(t)$] because the $^{176}Lu/^{177}Hf$ ratio of the depleted mantle is higher than chondritic values (Blichert-Toft and Albarède 1997; Kinny and Maas 2003). The second notable feature of the data is the large number of zircons that have negative $\varepsilon_{Hf}(t)$ values (as low as –6.2) (Figs. 5b, 6b). They could be produced by mixing between depleted mantle and enriched crustal derivatives, which would probably result in a broad range of initial isotope ratios from positive to negative, consistent with the enclave data (Figs. 5b, 6b). Therefore, we propose that the primary magma of the mafic enclaves was derived from a depleted mantle source.

In summary, in situ zircon U–Pb age and Hf isotopic data identify three sources that contributed to the origin of the Gudaoling granitoid: depleted mantle, crustally-derived magma and wall rocks (Archean gneiss).

## Magma mixing in the generation of granites

Zircons crystallizing in a melt retain a record of changes in ambient conditions during their growth. Consequently, they provide an insight into the dynamics of the magmatic system during a particular period of activity. The data and models presented here indicate that the individual rock types in the Gudaoling batholith represent varying degrees of hybridization between magmas derived from pre-existing crustal material and a depleted mantle-derived component.

Some zircons in the enclaves have similar CL patterns, U–Pb ages and Hf isotopic compositions to those in the host monzogranite. As stated previously, most mafic microgranular enclaves contain feldspar and quartz megacrysts that were derived from the host granites, and these, together with the zircons, were introduced by magma mingling. Besides these, other zircons in the enclaves have a large range of $\varepsilon_{Hf}(t)$ values (–6.2 to +4.5) (Figs. 5b, 6b). Zircons in the monzogranites also have a large range of $\varepsilon_{Hf}(t)$ values (Fig. 5a, 6a). The heterogeneous distribution of Hf isotopic compositions (Figs. 5, 6) cannot be indicative of a simple 'liquid line of descent' crystallization history, but instead indicates that two discrete magmas, one derived from pre-existing crustal material and the other from a depleted mantle-derived component, were involved in their genesis. The variable $\varepsilon_{Hf}(t)$ values of zircons in the enclaves and monzogranites also indicate a lack of equilibration during magma mixing.

The zircons in the enclaves with relatively dark, homogeneous CL patterns have relatively high $\varepsilon_{Hf}(t)$ values, while those with dark cores and lighter rims that are separated by irregular interfaces have low $\varepsilon_{Hf}(t)$ values (Fig. 3f). All these grains display resorption textures, clearly indicating that they were incorporated in and interacted with a magma with a low $\varepsilon_{Hf}(t)$ value. In contrast, zircons in the host monzogranites with high $\varepsilon_{Hf}(t)$ values (up to –15.1) clearly indicate that they were incorporated in and interacted with a magma with a high $\varepsilon_{Hf}(t)$ value. All these features indicate a mixing process of two magmas derived from different sources: a pre-existing crustal source and a depleted mantle-derived component. As discussed by Cherniak et al. (1995), Cherniak et al. (1997) and Cherniak and Watson (2000), zircon has a Lu–Hf closure temperature higher than the U–Pb isotopic system. Our results show that the mafic and felsic magmas mixed not only at low temperature as shown by whole-rock Sr and Nd isotopes, but also at high temperature (>800°C), which is consistent with the results of rheological calculations (Neves and Vauchez 1995). Rheological calculations indicate that viscosity and density contrasts pose no barrier to mixing basaltic (1,100°C) and granitic (800–900°C) magmas, provided they are moderately hydrous (Neves and Vauchez 1995).

In summary, the Gudaoling batholith is characterized by magma mixing. The variations in Hf isotopic compositions of zircons are the result of mingling and mixing between two parental magmas; one derived from a depleted mantle source and the other from pre-existing crustal material.

## Conclusions

1. Zircon U–Pb isotopic dating of the Gudaoling batholith yields an age of 120 ± 1 Ma for the mafic microgranular enclaves and an identical age of 120 ± 1 Ma for the host monzogranite. They are

indistinguishable within the analytical uncertainty, establishing that the mafic and felsic magmas were coeval. The presence of inherited zircons with older U–Pb ages and unradiogenic Hf isotopic compositions indicates some wall-rock contamination, but it was only minor.

2. The hafnium isotopic data establish that zircons in the Early Cretaceous Gudaoling monzogranite, its mafic microgranular enclaves and Archean gneissic wall rock have distinct characteristics, indicative of a lack of equilibration. This enables the identification of three sources that contributed to the origin of the granitoid: depleted mantle, crust-derived magma and wall rocks (Archean gneiss). One of the most important features is that a depleted mantle source contributed to the origin of the Gudaoling batholith, since this was not detected using conventional geochemical data nor was it evident in the Sr and Nd isotopic data for either the enclaves or the granites (Yang et al. 2004a). That zircon Hf isotopic data can establish that mafic microgranular enclaves were clearly mantle-derived opens up exciting new possibilities for studying the origin and compositional diversity of intermediate to felsic igneous rocks.
3. Zircon U–Pb dating and Hf isotopic compositions rule-out simple crystal-liquid fractionation or restite unmixing as the major genetic link between enclaves and host rocks. Instead, the variations in Hf isotopic compositions indicate that the Gudaoling granite-enclave assemblage was the result of mingling and high-temperature mixing between two parental magmas: the enclaves were derived from a depleted mantle source and the granite from pre-existing crustal material, coupled with minor assimilation of wall rocks.

**Acknowledgments** We are grateful to Drs. Hong-Lin Yuan, Chun-Rong Diwu and Shan Gao of the Key Laboratory of Continental Dynamics, Department of Geology, Northwest University, for assistance with collecting the analytical data. This work was financially supported by the National Science Foundation of China (NSFC grants 40325006 and 40203005) and ''Funds for 100 Outstanding Talents Plan''.

## References

Andersen T (2002) Correction of common lead in U–Pb analyses that do not report $^{204}$Pb. Chem Geol 192:59–79

Ballard JR, Palin JM, Williams IS, Campbell IH, Faunes A (2001) Two ages of porphyry intrusion resolved for the super-giant Chuquicamata copper deposit of northern Chile by ELA-ICM-MS and SHRIMP. Geology 29:383–386

Barbarin B (1990) Plagioclase xenocrysts and mafic magmatic enclaves in some granitoids of the Sierra Nevada Batholith, California. J Geophys Res 95:17747–17756

Barbarin B (2005) Mafic magmatic enclaves and mafic rocks associated with some granitoids of the central Sierra Nevada batholith, California: nature, origin, and relations with the hosts. Lithos 88:155–177

Blichert-Toft J, Albarède F (1997) The Lu–Hf geochemistry of chondrites and the evolution of the mantle-crust system. Earth Planet Sci Lett 148:243–258

Bonin B (2004) Do coeval mafic and felsic magmas in post-collisional to within-plate regimes necessarily imply two constrasting, mantle and crust, sources? A review. Lithos 78:1–24

Chappell BW (1997) Compositional variation within granite suites of the Lachlan Fold Belt: its causes and implications for the physical state of granite magma. Trans R Soc Edinb Earth Sci 88:159–170

Chappell BW, Stephens WE (1988) Origin of infracrustal (I-type) granite magmas. Trans R Soc Edinb Earth Sci 79:71–86

Chappell BW, White AJR, Wyborn D (1987) The importance of residual source material (restite) in granite petrogenesis. J Petrol 28:1111–1138

Chappell BW, White AJR, Williams IS, Wyborn D, Wyborn LAI (2000) Lachlan Fold Belt granites revisited: high- and low-temperature granites and their implications. Aust J Earth Sci 47:123–138

Chen YD, Price RC, White AJR, Chappell BW (1989) Inclusions in three S-type granites from southeastern Australia. J Petrol 30:1181–1218

Cherniak DJ, Watson EB (2000) Pb diffusion in zircon. Chem Geol 172:5–24

Cherniak DJ, Hanchar JM, Watson EB (1995) Hf and rare earth diffusion in zircon. EOS Trans Am Geophys Union 76:704

Cherniak DJ, Hanchar JM, Watson EB (1997) Diffusion of tetravalent cations in zircon. Contrib Mineral Petrol 127:383–390

Clynne MA (1999) A complex magma mixing origin of rock erupted in 1915, Lassen Peak, California. J Petrol 40:105–132

Didier J, Barbarin B (1991) Enclaves and granite petrology, developments in petrology. Elsevier, Amsterdam, p 625

Eberz GW, Nicholls IA, Maas R, McCulloch MT, Whitford DJ (1990) The Nd- and Sr-isotopic composition of microgranitoid enclaves and their host rocks from the Swifts Creek Pluton, southeast Australia. Chem Geol 85:119–134

Eichelberger JC (1980) Vesiculation of mafic magma during replenishment of silicic magma reservoirs. Nature 288:446–450

Elburg MA (1996) U–Pb ages and morphologies of zircon in microgranitoid enclaves and peraluminous host granites: evidence for magma mingling. Contrib Mineral Petrol 123:177–189

Goolaerts A, Mattielli N, de Jong J, Weis D, Scoates JS (2004) Hf and Lu isotopic reference values for the zircon standard 91500 by MC-ICP-MS. Chem Geol 206:1–9

Griffin WL, Pearson NJ, Belousova E, Jackson SE, van Achterbergh E, O'Reilly SY, Shee SR (2000) The Hf isotope composition of cratonic mantle: LAM-MC-ICPMS analysis of zircon megacrysts in kimberlites. Geochim Cosmochim Acta 64:133–147

Griffin WL, Wang X, Jackson SE, Pearson NJ, O'Reilly SY (2002) Zircon geochemistry and magma mixing, SE China: in-situ analysis of Hf isotopes, Tonglu and Pingtan igneous complexes. Lithos 61:237–269

Holden P, Halliday AN, Stephens WE (1987) Neodymium and strontium isotope content of microdiorite enclaves points to mantle input to granitoid production. Nature 330:53–56

Iizuka T, Hirata T. (2005) Improvements of precision and accuracy in in situ Hf isotope microanalysis of zircon using the laser ablation-MC-ICPMS technique. Chem Geol 220:121–137

Keay S, Collins WJ, McCulloch MT (1997) A three-component Sr–Nd isotopic mixing model for granitoid genesis, Lachlan fold belt, eastern Australia. Geology 25:307–310

Kemp AIS, Hawkesworth CJ (2003) Granitic perspectives on the generation and secular evolution of the continental crust. In: Rudnick RL (ed) The crust, treatise in geochemistry, vol 3, pp 349–410

Kemp AIS, Hawkesworth CJ (2006) Using hafnium and oxygen isotopes in zircons to unravel the record of crustal evolution. Chem Geol 226:144–162

Kepezhinskas P, McDemott F, Defant MJ, Hochstaedter A, Drummond MS, Hawkesworth CJ, Koloskov A, Maury RC, Bellon H (1997) Trace element and Sr–Nd–Pb isotopic constraints on a three-component model of Kamchatka Arc petrogenesis. Geochim Cosmochim Acta 61:577–600

Kinny PD, Maas R (2003) Lu–Hf and Sm–Nd isotope systems in zircon. In: Hanchar JM, Hoskin PWO (eds) Zircon. Rev Mineral Geochem 53:327–341

Kinny PD, Compston W, Williams IS (1991) A reconnaissance ion-probe study of hafnium isotopes in zircons. Geochim Cosmochim Acta 55:849–859

LBGMR (Liaoning Bureau of Geology and Mineral Resources) (1989) Regional Geology of Liaoning Province (in Chinese with English abstract). Geological Publishing House, Beijing

Lesher CE (1990) Decoupling of chemical and isotopic exchange during magma mixing. Nature 344:235–237

Lu XP, Wu FY, Lin JQ, Sun DY, Zhang YB, Guo LC (2004) Geochronological successions of the early Precambrian granitic magmatism in southern Liaodong Peninsula and its constraints on tectonic evolution of the North China Craton (in Chinese with English abstract). Chin J Geol 39:123–138

Ludwig KR (2003) ISOPLOT 3.0: a geochronological toolkit for microsoft excel, Berkeley Geochronology Center. Special publication no. 4

Luo Y, Sun M, Zhao GC, Li SZ, Xu P, Ye K, Xia XP (2004) LA-ICP-MS U–Pb zircon ages of the Liaohe Group in the Eastern Block of the North China Craton: constraints on the evolution of the Jiao-Liao-Ji Belt. Precam Res 134:349–371

Maas R, Nicholls IA, Legg C (1997) Igneous and metamorphic encalves in the S-type Deddick Granodiorite, Lachlan Fold Belt, SE Australia: petrographic, geochemical and Nd–Sr isotopic evidence for crustal melting and magma mixing. J Petrol 38:815–841

Millar IL, Willan RCR, Wareham CD, Boyce AJ (2001) The role of crustal and mantle sources in the genesis of granitoids of the Antarctic Peninsula and adjacent crustal rock. J Geol Soc Lond 158:855–867

Neves SP, Vauchez A (1995) Successive mixing and mingling of magmas in a plutonic complex of Northeast Brazil. Lithos 34:275–299

Pidgeon RT, Aftalion M (1978) Cogenetic and inherited zircon U-Pb systems in Palaeozoic granites of Scotland and England. In: Bowes DR, Leake BE (eds) Crustal processes and evolution in Northwestern Britain and adjacent regions. Geol J Spec Issue 10, pp 183–220

Poli G, Tommasini S, Halliday AN (1996) Trace elements and isotopic exchange during acid-basic magma interaction processes. Trans R Soc Edinb Earth Sci 87:225–232

Snyder D, Tait S (1998) The imprint of basalt on the geochemistry of silicic magmas. Earth Planet Sci Lett 160:433–445

Soderlund U, Patchett PJ, Vervoort JD, Isachsen CE (2004) The $^{176}$Lu decay constant determined by Lu–Hf and U–Pb isotope systematics of Precambrian mafic intrusions. Earth Planet Sci Lett 219:311–324

Sun SS, McDonough WF (1989) Chemical and isotopic systematics of oceanic basalts: implications for mantle composition and processes. In: Saunders AD, Norry MJ (eds) Magmatism in the Ocean Basins. Geol Soc Spec Publ 42:313–345

Vernon RH (1984) Microgranitoid enclaves: globules of hybrid magma quenched in a plutonic environment. Nature 304:438–439

Vernon RH, Etheridge ME, Wall VJ (1988) Shape and microstructure of microgranitoid enclaves: indicators of magma mingling and flow. Lithos 22:1–11

Wang X, Griffin WL, Wang Z, Zhou XM (2003) Hf isotope compositions of zircons and implications for the petrogenesis of Yajiangqiao granite, Hunan Province, China. Chin Sci Bull 48:995–998

White AJR, Chappell BW, Wyborn D (1999) Application of the restite model to the Deddick granodiorite and its enclaves—a reinterpretation of the observations and data of Mass et al. (1997). J Petrol 40:413–421

Woodhead J, Hergt J, Shelley M, Eggins S, Kemp R (2004) Zircon Hf-isotope analysis with an excimer laser, depth profiling, ablation of complex geometries, and concomitant age estimation. Chem Geol 209:121–135

Wu FY, Lin JQ, Wilde SA, Zhang XO, Yang JH (2005a) Nature and significance of the early Cretaceous giant igneous event in Eastern China. Earth Planet Sci Lett 233:103–119

Wu FY, Yang JH, Wilde SA, Zhang XO (2005b) Geochronology, petrogenesis and tectonic implications of the Jurassic granites in the Liaodong Peninsula, NE China. Chem Geol 221:127–156

Wu FY, Yang YH, Xie LW, Yang JH, Xu P (2006) Hf isotopic compositions of the standard zircons in U–Pb geochronology. Chem Geol (in press). DOI 10.1016/j.chemgeo.2006.05.003

Yang JH, Wu FY, Chung SL, Wilde SA, Chu MF (2004a) Multiple sources for the origin of granites: geochemical and Nd/Sr isotopic evidence from the Gudaoling granite and its mafic enclaves, NE China. Geochim Cosmochim Acta 68:4469–4483

Yang JH, Wu FY, Zhang YB, Zhang Q, Wilde SA (2004b) Identification of Mesoproterozoic zircons in a Triassic dolerite from the Liaodong Peninsula, Northeast China. Chin Sci Bull 49:1958–1962

Yang JH, Wu FY, Chung SL, Wilde SA, Chu MF (2006a) A hybrid origin for the Qianshan A-type granite, northeast China: Geochemical and Sr–Nd–Hf isotopic evidence. Lithos 89:89–106

Yang JH, Wu FY, Shao JA, Wilde SA, Xie LW, Liu XM (2006b) Constraints on the timing of uplift of the Yanshan Fold and Thrust Belt, North China. Earth Planet Sci Lett 246:336–352

Yuan HL, Gao S, Liu XM, Li HM, Gunther D, Wu FY (2004) Accurate U–Pb age and trace element determinations of zircon by laser ablation—inductively coupled plasma mass spectrometry. Geostand Newslett 28:353–370

Zhao GC, Wilde SA, Cawood PA, Sun M (2001) Archean blocks and their boundaries in the North China Craton: lithological, geochemical, structural and P–T path constraints and tectonic evolution. Precam Res 107:45–73

Zhao GC, Sun M, Wilde SA, Li SZ (2005) Late Archean to Paleoproterozoic evolution of the North China Craton: key issues revisited. Precam Res 136:177–202